ISBN: 978-3-95450-241-7 ISSN: 2673-5350 doi:10.18429/JACoW-IBIC2022-TU2T1

COLLIMATION AND MACHINE PROTECTION FOR LOW EMITTANCE RINGS*

J. Dooling†, Y. Lee, M. Borland, A. Grannan, C. Graziani, R. Lindberg, G. Navrotski
Argonne National Laboratory, Lemont, IL, USA
N. Cook, RadiaSoft, Boulder, CO, USA
D. Lee, University of California, Santa Cruz, CA, USA

Abstract

The reduced emittance and concomitant increase in electron beam intensity in Fourth Generation Storage Ring (4GSR) light sources lead to the challenging machine protection problem of how to safely dispose of the circulating charge during unplanned whole-beam loss events. Two recent experiments conducted to study the effects of 4GSR whole-beam aborts showed that damage to candidate collimator materials can be severe. This is a paradigm shift for SR light source machine protection. Typically the biggest threat to the machine is from CW synchrotron radiation. The choice of collimator material is important. High-Z, high-density materials such as tungsten may appear effective for stopping the beam in static simulations; however, in reality, short radiation lengths will cause severe destructive hydrodynamic effects. In our experiments, significant damage was observed even in low-Z aluminum. Thus unplanned, whole-beam aborts cannot readily be stopped in a single collimator structure. In this tutorial, alternatives such as multiple collimators and fan-out abort kicker systems will be discussed. Collimator design strategy and foreseen diagnostics for their operation will also be presented.

INTRODUCTION

The ultra-low emittance, high-intensity electron beams in Fourth Generation storage ring (4GSR) machines are capable of causing high-energy-density (HED) interactions on technical surfaces such as collimators or vacuum chamber walls. HED is defined as energy densities exceeding roughly 10^{11}J/m^3 [1]. Dose is defined as absorbed energy per unit mass, $D = E_a/\rho$. HED conditions represent an acute dose of 37 MGy in aluminum, 11.2 MGy in copper, and 5.2 MGy in tungsten. The term "acute" is somewhat ambiguous; here it implies the duration of the deposition is short. A useful rule-of-thumb is to compare the duration with a thermal diffusion time defined from the heat equation as $\tau_D = L^2/\alpha$, where L is a characteristic scale length of the absorbed energy distribution and α is the diffusivity. For systems undergoing rapid temperature or phase changes, α is a complex function of dose and time. For example, diffusivity and thermal conductivity change significantly in aluminum as the material changes from solid to liquid phase [2]. Thermal conductivity falls further if the collimator enters a warm dense matter (WDM) regime [3]. Hence, sophisticated, self-consistent analysis may be required to properly capture material evolution under incident dose.

MACHINE PROTECTION

Third-generation storage ring light sources have typically not focused on protecting accelerator hardware from loss of the circulating electron beam; the effort has been and is still centered on protecting components from x-ray photons. Some measures have been taken such as shielding undulator permanent magnets from accumulated dose caused by high-energy electromagnetic showers; however, this exposure takes place over weeks and months and is not mechanically destructive. Attention to synchrotron photons is warranted given that insertion device beam lines generate kilowatts of beam power with power densities up to 600 kW/mrad^2 [4].

The Advanced Photon Source Upgrade (APS-U) Final Design Report (FDR) [4] states, "The machine protection system (MPS) protects the APS storage ring vacuum system from x-ray beam heating, loss of water cooling, and elevated vacuum levels." On the other hand, documentation for high-energy experimental facilities such as the Electron Ion Collider (EIC) explicitly discuss the need for MPS to protect against beam strikes [5], "...the primary goal of the MPS is to protect the EIC accelerators from the possible damage caused by electron and proton beams."

Two experiments conducted in the APS storage-ring (SR) [6] have led to the understanding that disposal of the electron beam during a whole beam dump—both planned and unplanned—must also be included in the function of the APS-U MPS. This language has been added to the MPS engineering specification document.

In the following subsections, we present a brief overview of MPS realizations at several accelerator facilities including APS-U. The selection is by no means comprehensive.

APS-U, Argonne National Laboratory

A schematic of the APS-U MPS topology is presented in Fig. 1. Twenty local MPS (LMPS) modules distributed around the ring feed the main MPS unit in the Main Control Room (MCR). Block diagrams for the logic paths are presented in Fig. 2. The top schematic depicts the Main logic block and the lower the local logic. Important subsystems to the MPS include the Front End Equipment Protection System (FE-EPS). The hierarchical architecture is common to

* This research used resources of the Advanced Photon Source (APS), one of the five U.S. Department of Energy (DOE) Office of Science user facilities and is based on work supported by Laboratory Directed Research and Development (LDRD) funding from Argonne National Laboratory, provided by the Director, Office of Science, of the U.S. DOE under Contract No. DE-AC02-06CH11357.
† dooling@anl.gov

ISBN: 978-3-95450-241-7 ISSN: 2673-5350 doi:10.18429/JACoW-IBIC2022-TU2T1

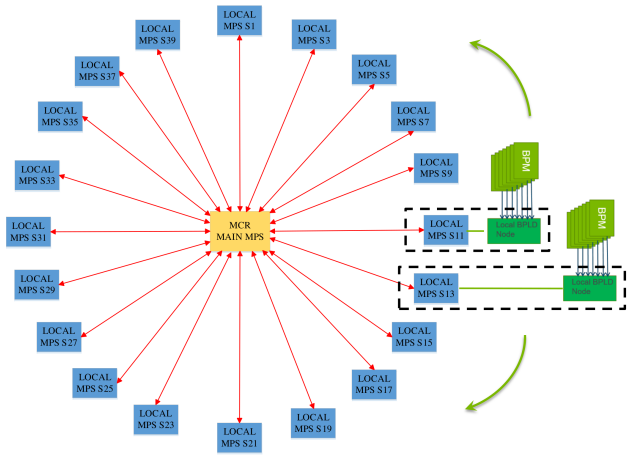

Figure 1: APS-U MPS topology.

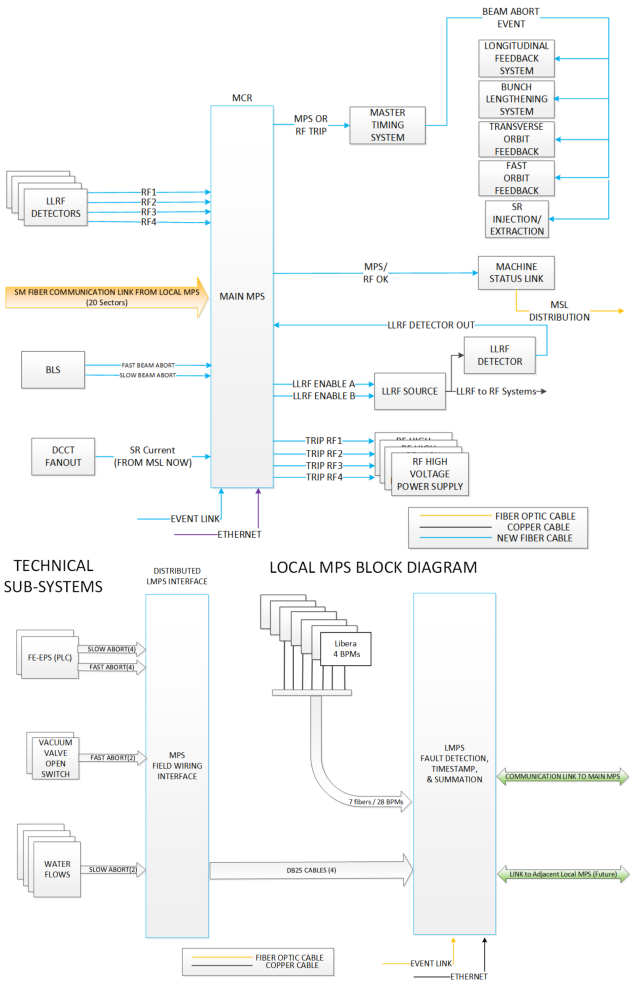

Figure 2: Logic diagrams for the main (top) and local MPS blocks (bottom). BLS stands for the bunch lengthening system.

many MPS configurations at other large laboratories, including those discussed below. For comparative purposes, the stored energy is 4.4 kJ and the average power is 1.2 GW if lost in one turn in the APS-U SR with 200 mA of circulating charge at 6 GeV.

EIC, Brookhaven National Laboratory

The EIC [7] will employ separate dedicated dump lines to terminate both proton and electron beams [5]. For the protons, the existing line for the Relativistic Heavy Ion Collider (RHIC) will be used, whereas a new line is planned for the electrons. The MPS must also protect against synchrotron x-ray photons. For operations at 10 GeV, the 3.834 km circumference electron ring stores 1160 bunches of 27.5 nC. Stored energy for this fill pattern is 320 kJ and average circulating power is 25 GW.

Proton Improvement Plan II, Fermilab

The Proton Improvement Plan II (PIP-II) at Fermilab will operate an 800 MeV superconducting linac at a current of 2 mA [8]. Operations are scheduled to begin in 2028. Four levels of protection are provided by the PIP-II MPS. First, the main level of protection comes from four upstream locations near the ion source utilizing four pairs of current sensitive devices: two pairs of ring pick ups and two pairs of scrapers. The second layer detects local beam losses in the medium energy beam transport (MEBT) line. The third level involves tracking readiness status from various subsystems such as RF, vacuum, and water. Finally, various configurations are considered including beam intensity, fill pattern, and destination [9].

Spallation Neutron Source, Oak Ridge National Laboratory

The Spallation Neutron Source (SNS) is a user facility operating a high-power proton beam. The purpose of the 1.4 MW proton beam is to strike a heavy metal target for neutron production. Similar to the APS, it must operate continuously for days at a time with periodic breaks for maintenance and studies, making reliability and up-time paramount. The SNS MPS has gone through a number of changes since first operations in 2006 [10–12]. Presently, the Fast Protection System (FPS), responsible for terminating beam, is being upgraded in a staged process [13]. The process starts with the Master MPS and Ring to Target Beam Transfer line (RTBT) components. Next, the Medium Energy Beam Transport (MEBT) and the coupled-cavity linac (CCL) systems will be addressed, followed by the injection dump and linac, and finally the Extraction Dump.

STRATEGY FOR PROTECTION OF APS-U CHAMBERS AND COLLIMATORS

The APS-U MPS system includes beam-position-limits detectors (BPLDs) that will abort the beam if the orbit exceeds defined amplitude or slope. The initial motivation for this system was to protect against damage to vacuum chambers from synchrotron radiation, which might bypass a radiation absorber if the orbit is large. In light of damage seen to APS collimators and to materials such as aluminum

ISBN: 978-3-95450-241-7 ISSN: 2673-5350 doi:10.18429/JACoW-IBIC2022-TU2T1

in APS experiments, it was realized that the BPLD system should also be configured to protect components from electron beam strikes. To understand the requirements, computer simulations of beam aborts in the presence of orbit distortion were performed with `elegant` [14, 15]. The simulations include models of the APS-U rf systems and cavities, including beam-loading, which significantly affects the rate of energy loss per turn when the rf systems trip (as they do for a beam abort). We modeled an uncontrolled orbit by ramping up the strength of one or more steering magnets, with the ramping rate determined by the power supply limit for the APS-U fast correctors. This simulates runaway fast orbit feedback. The rf drive was then muted when the orbit distortion at the relevant BPMs exceeded a threshold value. Simulations were performed for various threshold values and evaluated in terms of whether particle losses were seen outside the whole-beam dumps. We found that, in order to prevent such losses, the interlock level should be ± 2 mm in the horizontal plane and ± 1.5 mm in the vertical plane. In both cases, the interlocks can be imposed only at the two BPMs per sector that have the largest beta function. These thresholds are comparable to those needed to protect the chamber from synchrotron radiation.

APS-U incorporates identical beam dumps in five consecutive sectors. Simulations show that, even in the presence of errors, the identical beam dumps reduce the probability of missing the dumps to less than 1%. Since we anticipated that the APS-U whole-beam dumps will be damaged over time, they are designed to be serviced without breaking ring vacuum, thanks to a load-lock system and removable surface pieces. Even so, it is desirable to reduce damage in order to increase the service interval and, more importantly, to reduce the chance that gradual erosion of the dump surfaces would lead to beam strikes in unwanted locations. Toward this end, we are incorporating a fan-out kicker (FOK) into the APS-U. This kicker will be fired when an rf system trips (or is commanded to trip). The FOK pulse duration will be one revolution period, with a half-sinusoidal shape, so that different bunches are kicked by different amounts. The idea is to disperse the bunches across the dump surface vertically and decrease the energy density, to either reduce or eliminate damage. Simulations with `elegant` show that if the kick amplitude does not exceed 200 µrad, there are no losses except at the beam dumps. For this kick amplitude, the maximum dose in aluminum is less than 2 MGy which is well below the damage threshold.

Another advantage of the FOK is that it has the potential to reduce the energy density sufficiently so that using copper for the beam dump surface may become an option. (Copper has a lower damage threshold than aluminum because of its comparatively poor heat capacity.) This is desirable because copper's higher Z (than aluminum) would result in better localization of the losses.

The use of the FOK for machine protection is complicated by the desire to use it for diagnostics purposes, primarily measurement of the vertical-plane dynamic acceptance. Simulations show that, if the orbit is well controlled, use of the FOK as a diagnostic is safe up to 30 mA stored current, in which case the beam hits a whole-beam dump. If the orbit is not well controlled, as might happen in early commissioning before the BPLDs are active and before the lattice is well tuned, the limit is reduced to 3.5 mA since a strike on a copper photon absorber is then a possibility.

APS-U will operate in on-axis swap-out mode [16, 17] at 200 mA with as few as 48 bunches, entailing disposal of single 15.3 nC bunches at the swap-out dump. Unlike the beam striking the whole-beam dumps, a swapped-out bunch is lost in a few hundred picoseconds, meaning that thermal diffusion does not help to diffuse the effect. In the original vertical-plane injection scheme [18], the beam would strike the dump surface at near-normal incidence, resulting in doses sufficient to melt aluminum. To prevent damage to the dump, we incorporated a decoherence kicker (DK) [19], that will be fired at least 200 turns prior to the swap-out event. This kicker will use a fast pulser similar to the pulsers used for injection, so it will only significantly affect the bunch being replaced. We have since switched to a horizontal-plane injection scheme that allows for a very gradual taper on the swap-out dump, so the dose is greatly reduced. However, should an injection/extraction kicker misfire, the bunch may impact other components with a less glancing angle. As a result, the DK is still considered essential. The DK waveform is monitored so that the injection/extraction kickers will not fire if the DK does not fire as required.

COUPLED CODE SIMULATIONS

We have begun to model the damage that unplanned and unprotected beam losses will have on accelerator components and materials in the APS-U SR [20, 21].

Figure 3 presents a dose map composed of multi-turn loss distributions derived from `elegant` simulations and measurements from a 200 mA beam dump described in Ref. [6]. The loss distributions are then used in MARS [22]

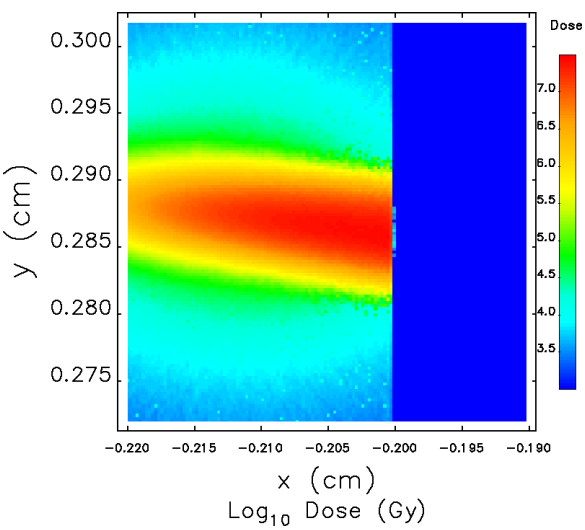

Figure 3: Multi-turn dose map from a 200 mA beam dump. The region $x < 0.2$ cm is aluminum and vacuum otherwise.

ISBN: 978-3-95450-241-7 ISSN: 2673-5350 doi:10.18429/JACoW-IBIC2022-TU2T1

Table 1: Thermal Properties

	c_p (J/(kg-K))	c_l (J/(kg-K))	T_1 (K)	T_m (K)	T_v (K)	ΔH_f (J/kg)	ΔH_v (J/kg)	D_v (J/kg≡Gy)
Aluminum	900	1138	293	933	2743	3.21×10^5	1.14×10^7	1.434×10^7

to generate the dose map. This distribution assumes the collimator surface remains intact during the beam dump. However, we have seen that the assumption is not the case during loss studies.

The MARS-generated dose map is passed to the FLASH code. FLASH [23] is a magnetohydrodynamics (MHD) based multi-physics code with a broad range of user communities among astrophysicists and plasma physicists. We use FLASH to simulate the collimator damage and the plasma evolution due to the beam strikes, making careful numerical assumptions to *emulate* the solid-state material and its phase change, both of which have limited scopes of implementations in FLASH.

FLASH assumes that every material inside the simulation domain is an inviscid compressible fluid. Without considering electromagnetic effects, the hydrodynamics properties are updated by solving the conservative form of Euler equations,

$$\begin{aligned} \frac{\partial \rho}{\partial t} + \nabla\cdot(\rho\mathbf{v}) &= 0, \\ \frac{\partial \rho\mathbf{v}}{\partial t} + \nabla\cdot(\rho\mathbf{v}\mathbf{v}) + \nabla P &= 0, \\ \frac{\partial \rho E}{\partial t} + \nabla\cdot[(\rho E + P)\mathbf{v}] &= 0, \end{aligned} \tag{1}$$

where ρ is the fluid density, $\mathbf{v} = (u, v, w)$ is the fluid velocity, and P is the thermal pressure. The total energy E is the sum of the internal energy and kinetic energy per unit mass,

$$E = \epsilon + \frac{1}{2}|\mathbf{v}|^2. \tag{2}$$

The pressure P and the temperature T are obtained by calculating the equation of states (EOS), where we rely on precalculated tabulated EOS data. FLASH will read the tabulated EOS data with given internal energy and density as,

$$P, T = \mathrm{EOS}(\rho, \epsilon). \tag{3}$$

We utilize FLASH's multi-temperature model that handles pressure, temperature, and internal energy separately for ions and electrons, which are not necessarily equal in high-energy-density plasmas. In other words, FLASH calculates Eqs. (1) and (3) separately for ions ($P_{\mathrm{ion}}, \epsilon_{\mathrm{ion}}, T_{\mathrm{ion}}$) and electrons ($P_{\mathrm{ele}}, \epsilon_{\mathrm{ele}}, T_{\mathrm{ele}}$), and computes the heat exchanges between electrons and ions through collisions.

The input energy dose map from the MARS simulation results will be added to the electron's internal energy (i.e., $\epsilon_{\mathrm{ele}} = \epsilon_{\mathrm{ele}} + E_{\mathrm{MARS}}$). This energy increment will be translated into the temperature rises at the collimator regions. FLASH will perform the thermal diffusion calculations by solving the isotropic diffusion equation as

$$\rho c_v \frac{\partial T}{\partial t} = \nabla\cdot K\nabla T, \tag{4}$$

where c_v is the specific heat at constant volume, and K is the thermal conductivity. Again, the multi-temperature model solves Eq. (4) for both ions and electrons separately, although we use electrons' thermal diffusion only, assuming that the electrons are the primary energy carrier.

FLASH provides several models to calculate the electron's thermal conductivity, K_{ele}, for plasma materials. For example, the Spitzer conductivity model [24] follows

$$K_{\mathrm{ele}} = \left(\frac{8}{\pi}\right)^{3/2} \frac{k_B^{7/2}}{e^4\sqrt{m_{\mathrm{ele}}}} \left(\frac{1}{1+3.3/\bar{z}}\right) \frac{T_{\mathrm{ele}}^{5/2}}{\bar{z}\ln\Lambda_{ei}}, \tag{5}$$

where k_B is the Boltzmann constant, e is the electron charge, m_{ele} is the mass of an electron, $\bar{z}$ is the average ionization level, and $\ln\Lambda_{ei}$ is the Coulomb logarithm associated with electron-ion collisions.

We should note that the model described in Eq. (5) is only valid for an ionized gas. In the case of solid-state matter (i.e., the collimator), we need to use a different approach for calculating the thermal conductivity. Currently, we are using a constant thermal conductivity (e.g., $2.05\times10^2\ \mathrm{Wm^{-1}K^{-1}}$ for aluminum) inside the collimator.

Alongside the different approaches for the thermal conductivity calculations inside the collimator region, we need to take care when updating physical quantities inside the collimator regions, as FLASH considers everything as a compressible fluid. Our strategy to *emulate* a solid-state matter and its phase transition are to utilize the `bdry_var` switch provided in FLASH.

FLASH offers the functionality of immersing a stationary physical boundary within the simulation domain, tagged as `bdry_var`. If a cell is tagged as `bdry_var`, then FLASH omits the hydrodynamics updates (i.e., neglects to solve Eq. (1)) to force the physical quantities at the cell to remain stationary. We initially tag the `bdry_var` of all the cells inside the collimator regions and let FLASH calculate only the thermal diffusion with a constant conductivity, expressed in Eq. (4). With this approach, we expect to see dispersion of the electron beam dose due to thermal conduction. In order to emulate the phase transition, we turn off the `bdry_var` if a cell reaches a threshold temperature. With `bdry_var` turned-off, FLASH will assume the cell is an inviscid compressible gas fluid vaporized from the solid collimator state.

This simplified two-phase model in our simulations introduces two main issues: determining the phase-transition threshold value and simulating the liquid-state matter. One

ISBN: 978-3-95450-241-7 ISSN: 2673-5350 doi:10.18429/JACoW-IBIC2022-TU2T1

possible method to determine the threshold value is to use the boiling temperature for the collimator material. However, this implies that FLASH calculates EOS for the solid-state matter correctly. As our current EOS data is only applicable for plasma, we have to use an arbitrary threshold value by considering it as a hyperparameter. In the case of the aluminum collimator, we configured the threshold value as 4115 K by benchmarking the trench formation patterns observed in the experimental results reported in [6]. It should be noted that the value 4115 K is just an interim value, and we expect a more accurate configuration once we improve the EOS models for the solid-state matter.

We also need to contemplate the liquid state during the phase transition to capture the collimator deformation more correctly. In our recent experiments reported in [6], we observed irregular-shaped collimator deformation, which is not captured in our FLASH simulations. We believe this is due to the lack of liquid state calculations in our current FLASH simulation setups. To help obtain a succinct idea of the liquid state contribution to the trench formation in the collimator, we took a heuristic strategy of performing the simulation by lowering the threshold value at the end of beam loss. This result is displayed in the right panel of Fig. 4. Obviously, a far more detailed analysis of the material properties is required to model the fluid dynamics in this situation properly. We will explore such options in our future study.

A 3-D microscopy view of a section of aluminum struck by a 200 mA, 6 GeV electron beam during collimator irradiation studies mentioned above is presented in Fig. 5. The melt channel is approximately 200 µm wide and 50 µm deep. Presumably a significant melt region lies below the channel surface [25]. Melted, expelled aluminum lines the channel above the collimator surface. We note that not every struck region looks like Fig. 5. Some have sharper, deeper walls similar to the simulation shown in Fig. 4 left.

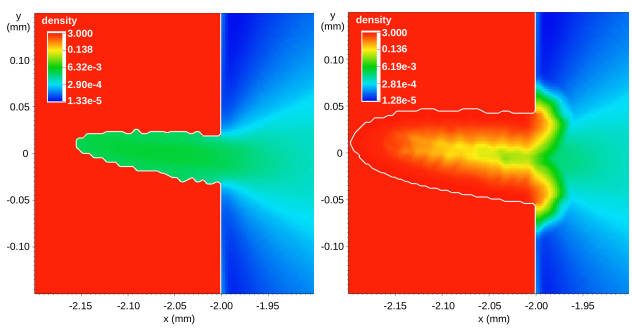

Figure 4: Allowing the release condition to jump from 4115 K to 2743 K at the end of energy deposition. In both frames, the white curve indicates the release boundary. Left: Density prior to the change in the release condition. Right: Density 5 ns after the release temperature threshold jump. The material within the new boundary is now a low-temperature plasma that may emulate a *liquid phase* region.

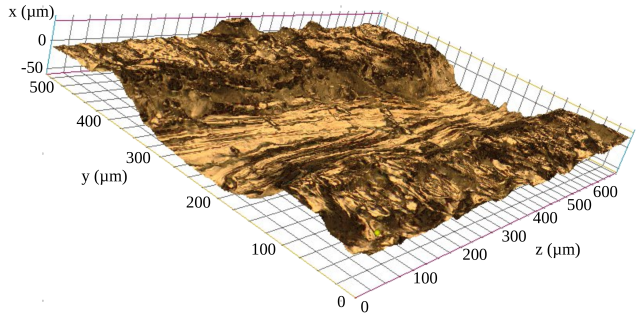

Figure 5: 3-D microscopy image showing the region of an aluminum collimator test piece struck by a 200 mA, 6 GeV beam dump.

DISCUSSION

We can perform a naive calculation of dose to give a general idea of the state of the irradiated material. Ignoring thermal diffusion, complete vaporization should take place for a specific energy or dose, D, if the following is true,

$$D \geq c_p(T_m - T_1) + \Delta H_f + c_l(T_v - T_m) + \Delta H_v, \quad (6)$$

where c_p is the specific heat at constant pressure, c_l the specific heat for liquid, T_m the melting temperature, T_1 the starting temperature, and T_v the vaporization temperature. ΔH_f and ΔH_v are the heat of fusion and heat of vaporization enthalpies. Assigning D_v the equality condition, Table 1 gives these values for aluminum. Thus, complete vaporization requires a dose of 14.34 MGy. The release condition shown in Fig. 4 left, $1.5T_v$ or 4115 K, corresponds to a dose of 4.83 MGy and notionally places material into a mixed-phase regime. The specific energy required to take the material to the fully melted condition without vaporization (ignoring ΔH_v) is 2.94 MGy. Rapid thermal expansion of the material will occur during this process, even without vaporization, which may also contribute to expulsion of material.

SUMMARY

Machine Protection Systems play a key role in assuring the reliability and sustainability of their respective accelerator facilities. In large facilities, MPS is implemented in hierarchical structures. Both hadron and electron beams are capable of mechanically damaging accelerator hardware. Work is underway to model the effects of beam strikes on accelerator hardware by coupling codes that simulate particle dynamics, particle-matter interactions, and hydrodynamic effects. Our initial results show promise when comparing simulations with experimental data.

ACKNOWLEDGEMENTS

For MPS information, special thanks to M. Smith and H. Bui of APS Argonne National Laboratory (ANL), A. Warden of PIP-II Fermilab, A. Drees. of EIC/RHIC Brookhaven National Laboratory, and A. Justice of SNS Oak Ridge National Laboratory. For assistance with analysis scripts, thanks also to R. Soliday and H. Shang of APS ANL.

ISBN: 978-3-95450-241-7 ISSN: 2673-5350 doi:10.18429/JACoW-IBIC2022-TU2T1

REFERENCES

[1] R. P. Drake, *Introduction to High-Energy-Density Physics*. Springer International Publishing, 2018. doi:10.1007/978-3-319-67711-8_1

[2] M. Leitner, T. Leitner, A. Schmon, K. Aziz, and G. Pottlacher, "Thermophysical Properties of Liquid Aluminum," *Metall. Mater. Trans. A*, vol. 48A, pp. 3036–3045, 2017. doi:10.1007/s11661-017-4053-6

[3] A. McKelvey *et al.*, "Thermal conductivity measurements of proton-heated warm dense aluminum," *Sci. Rep.*, vol. 7, no. 7015, pp. 1–10, 2017. doi:10.1038/s41598-017-07173-0

[4] "Advanced Photon Source Upgrade Project Final Design Report," Advanced Photon Source, Argonne National Laboratory, Tech. Rep., 2019. https://publications.anl.gov/anlpubs/2019/07/153666.pdf

[5] S. Seletskiy and A. Drees, "Electron ion collider machine protection system: Requirements for an electron storage ring abort system," Electron-Ion Collider, Brookhaven National Laboratory, Tech. Rep., 2020. https://technotes.bnl.gov/PDF?publicationId=222327

[6] J. Dooling *et al.*, "Collimator irradiation studies in the argonne advanced photon source at energy densities expected in next-generation storage ring light sources," *Phys. Rev. Accel. Beams*, vol. 25, no. 4, p. 043 001, 2022. doi:10.1103/PhysRevAccelBeams.25.043001

[7] C. Montag, "eRHIC - an Electron-Ion Collider at BNL," Collider Accelerator Department, Brookhaven National Laboratory, Tech. Rep., 2018. https://www.osti.gov/servlets/purl/1566296

[8] S. Nagaitsev and V. Lebedev, "A cost-effective upgrade path for the fermilab accelerator complex," Tech. Rep., 2021. doi:10.48550/arXiv.2111.06932

[9] A. Warner *et al.*, "Machine Protection System Research and Development for the Fermilab PIP-II Proton Linac," in *Proc. ICALEPCS'17*, Barcelona, Spain, Oct. 2017, pp. 1643–1645. doi:10.18429/JACoW-ICALEPCS2017-THPHA110

[10] C. S. III, D. J. Armstrong, A. Jones, T. A. Justice, and D. H. Thompson, "The SNS Machine Protection System: Early Commissioning Results and Future Plans," in *Proc. PAC'05*, Knoxville, TN, USA, May 2005. https://jacow.org/p05/papers/RPPE021.pdf

[11] S. W. Lee, J. A. Ball, M. T. Crofford, T. L. Davidson, T. W. Hardek, and S. L. Jones, "Spallation Neutron Source High-Power Protection Module Test Stand," in *Proc. LINAC'10*, Tsukuba, Japan, Sep. 2010, pp. 262–264. https://jacow.org/LINAC2010/papers/MOP089.pdf

[12] A. P. Zhukov, "Experience with the SNS Loss Monitoring and Machine Protection," in *Proc. NAPAC'13*, Pasadena, CA, USA, Sep.-Oct. 2013, pp. 714–718. https://jacow.org/PAC2013/papers/WEYA2.pdf

[13] T. A. Justice, personal communication, 2022.

[14] M. Borland, "elegant: A Flexible SDDS-Compliant Code for Accelerator Simulation," Advanced Photon Source, Tech. Rep. LS-287, 2000. http://www.aps.anl.gov/Science/Publications/lsnotes/ls287.pdf

[15] Y. Wang and M. Borland, "Implementation and Performance of Parallelized Elegant," in *Proc. PAC'07*, Albuquerque, NM, USA, Jun. 2007, pp. 3444–3446. https://jacow.org/p07/papers/THPAN095.pdf

[16] R. Abela, W. Joho, P. Marchand, S. V. Milton, and L. Z. Rivkin, "Design Considerations for a Swiss Light Source (SLS)," in *Proc. EPAC'92*, Berlin, Germany, Mar. 1992, pp. 486–489.

[17] L. Emery and M. Borland, "Upgrade Opportunities at the Advanced Photon Source Made Possible by Top-Up Operations," in *Proc. EPAC'02*, Paris, France, Jun. 2002. https://jacow.org/e02/papers/TUALA003.pdf

[18] A. Xiao and M. Borland, "Transport Line Design and Injection Configuration Optimization for the Advanced Photon Source Upgrade," in *Proc. IPAC'18*, Vancouver, Canada, Apr.-May 2018, pp. 1287–1289. doi:10.18429/JACoW-IPAC2018-TUPMF017

[19] M. Borland, J. C. Dooling, R. R. Lindberg, V. Sajaev, and A. Xiao, "Using Decoherence to Prevent Damage to the Swap-Out Dump for the APS Upgrade," in *Proc. IPAC'18*, Vancouver, Canada, Apr.-May 2018, pp. 1494–1497. doi:10.18429/JACoW-IPAC2018-TUPMK004

[20] J. C. Dooling *et al.*, "Simulations of Beam Strikes on Advanced Photon Source Upgrade Collimators using FLASH, MARS, and elegant," in *Proc. IPAC'21*, Campinas, Brazil, May 2021, pp. 2562–2565. doi:10.18429/JACoW-IPAC2021-WEXC04

[21] J. C. Dooling *et al.*, "Hydrodynamic and Beam Dynamic Simulations of Ultra-Low Emittance Whole Beam Dumps in the Advanced Photon Source Storage Ring," Albuquerque, New Mexico, USA, Aug. 2022, presented at NAPAC'22, Albuquerque, New Mexico, USA, Aug. 2022, paper TUPA21, to be published.

[22] N. V. Mokhov, "The Mars Code System User's Guide," Fermilab, FN 628, 1995.

[23] B. Fryxell *et al.*, "FLASH: An adaptive mesh hydrodynamics code for modeling astrophysical thermonuclear flashes," *Astrophys. J. Suppl. Ser.*, vol. 131, no. 1, pp. 273–334, 2000. doi:10.1086/317361

[24] S. Atzeni and J. Meyer-ter-Vehn, *The physics of inertial fusion: beam plasma interaction, hydrodynamics, hot dense matter*. OUP Oxford, 2004.

[25] J. C. Dooling *et al.*, "Diagnostics for Collimator Irradiation Studies in the Advanced Photon Source Storage Ring," in *Proc. IBIC'20*, Santos, Brazil, Sep. 2020, pp. 26–33. doi:10.18429/JACoW-IBIC2020-TUAO02